Preliminary study of EEHG-based superradiant undulator radiation at the HLS-II storage ring *

Wei-Wei Gao(高巍巍)[1;1)]   He-Ting Li(李和廷)[2]   Lin Wang(王琳)[2]

[1] College of Mathematics and Physics, Fujian University of Technology, Fuzhou 350118, China
[2] National Synchrotron Radiation Laboratory, University of Science and Technology of China, Hefei 230029，China

Abstract: We investigate storage ring-based Echo-Enabled Harmonic Generation (EEHG) superradiant undulator radiation as a possible scheme to obtain shorter wavelengths at the HLS-II (Hefei Light Source-II) storage ring. In this paper we give the designation of the storage ring based EEHG up to the 26th harmonic, where 31 nm vacuum ultraviolet light is radiated from an 800 nm seeded laser. The novelty of our design is that both the two dispersion sections of EEHG are realized by the storage ring's own magnet structure. In particular, the whole ring is used as the first dispersion section, and two modulators of the traditional EEHG can be done with the same undulator. These two dispersion sections are realized by changing the superperiod of the present lattice structure, and more precisely by changing the focusing strengths of the present structure. Since no additional magnets and chicanes are used, the beam circulates around the storage ring repeatedly, and thus this storage ring-based EEHG can have a higher repetition rate than a linac-based EEHG.

1   Introduction

The recently proposed double modulator free electron laser scheme, called the Echo-Enabled Harmonic Generation (EEHG) scheme [1], can generate high harmonic modulation with small energy modulation. Also, the EEHG has remarkable features in that the bunching factor decays slowly with the harmonic number and the high frequency up-conversion efficiency. Until now, all EEHG free electron laser experiment results have been based on linear accelerators, and have achieved remarkable results. Examples include SLAC's NLCTA [2–5], and the Shanghai Deep Ultraviolet Free-Electron Laser facility (SDUV) [6].

Several ways have been proposed to produce radiation at short wavelengths in storage rings. In this paper we carried out a simulation of a storage ring-based EEHG scheme at the Hefei Light Source-II (HLS-II) storage ring for vacuum ultraviolet radiation. Compared to the UV radiation derived from organic interactions, the pulse structure of FEL radiation can be designed according to the user's needs. In addition, it can be continuously adjusted over a large range. The UV radiation produced by this method can be widely used in photo-etching, photo-ionization and other applications in industry. Particularly, the excitation wavelengths of most molecules and radicals are in the vacuum ultraviolet wavelength range. Therefore, vacuum ultraviolet waves are superior in probe experiments for gas phase atoms, and molecular and surface physics.

Previously, the possibility of a storage ring-based EEHG FEL scheme was investigated at some synchrotron radiation facilities, such as DELTA [7] and SOLEIL [8]. The highlight of our research is that we designed a storage ring-based EEHG superradiant undulator radiation without rearranging the magnets or adding chicanes. The EEHG is realized by a newly designed low momentum compaction factor lattice, which is obtained by changing the focusing strengths as well as the symmetry property.

A draft schematic of the storage ring-based EEHG superradiant undulator radiation at HLS-II is given in Fig. 1.

As shown in the diagram, a new storage ring lattice is designed and there are no other insertion devices except the modulator and radiator used for the EEHG superradiant undulator radiation setup. Similar to the normal operation mode, the electron beam is injected in top-up injection mode and circulates around the storage ring at 800 MeV. After several damping times, the modulator is

turned on and the seeded laser interacts with the electron beam at modulator 1. Then the beam passes through the whole storage ring, which can be considered as chicane 1 of the classical EEHG scheme. The beam is then sent to the modulator again. At this moment, the laser power is changed from modulator 1 and can be considered as modulator 2. The two modulation lasers with the same frequency are provided by splitting one laser beam. The two modulation lasers may have different power, which can be adjusted by the attenuation controller. In this operation set up, we have to control the time interval between the two lasers to be exactly equal to the revolution period of the modulated bunches. After passing through modulator 2, the beam proceeds to dispersion 2, which is part of the storage ring lattice. Finally, the beam emits at the n-th harmonic of the seeded laser at the radiator.
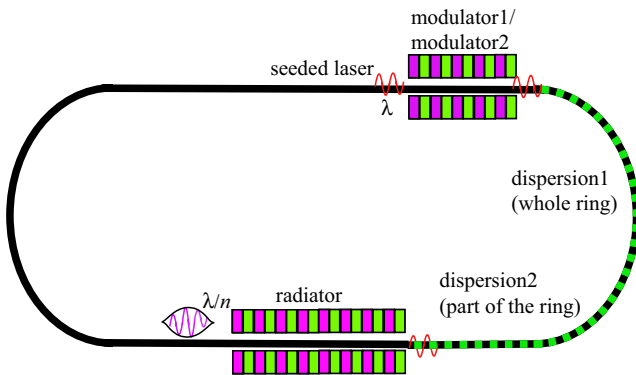

Fig. 1. (color online) Schematic diagram of storage-based EEHG superradiant undulator radiation. The seeded laser interacts with the beam at modulator 1, and passes through dispersion 1 (whole ring), then enters into modulator 2 (actually the same undulator as modulator 1); after that it goes through dispersion 2 (part of the ring), and finally radiates at the n-th harmonic of the seeded laser.

The HLS-II storage ring is a DBA lattice composed of four super-periods. It is a small synchrotron light source with a circumference of 66.1308 m. The main parameters of HLS-II are given in Table 1.

Table 1.   Parameters of the HLS-II storage ring.

parameter	value
circumference/m	66.1308
energy/MeV	800
total beam current/mA	350
momentum compaction factor	0.0205
RF voltage/kV	250
RF frequency/MHz	204

As follows from Table 1, the repetition rate of the electron beam in the HLS-II storage ring is 204 MHz with

45 bunches filled in, and 4.533 MHz with only one bunch filled in. We can choose one or some bunches of the 45 buckets to generate EEHG according to the seeded laser's repetition rate. The repetition rate of the seeded laser must be an integer number of times of the electron's revolution frequency. But, regardless of whether one bunch filled mode or multiple bunches filled mode is used, the repetition rate of EEHG is of the order of 1–100 MHz. Hence, the storage ring-based EEHG scheme may have a higher repetition rate than linac-based EEHG, which at the level of 100 Hz to 1 MHz (see e.g.[9, 10]).

For an electron storage ring the whole ring's linear matrix element R_{56} is approximately proportional to the circumference (see Eq. (1)),

$$R_{56} = \alpha C, \qquad (1)$$

where α is the momentum compaction factor and C is the circumference.

As a result, the matrix element R_{56} can be easily reduced for small storage rings compared to large rings. Thus the HLS-II storage ring has the potential option of the whole ring being used as the first dispersion section.

In this paper we systematically study the storage-based EEHG scheme. First, theoretical analysis of the storage ring-based EEHG scheme as well as the required storage ring parameters are presented. In Section 3 we design storage ring parameters for EEHG superradiant undulator radiation at HLS-II by changing the quadrupole strengths and keeping the magnet positions the same as in the present structure. We demonstrate the performance of the HLS-II storage-based EEHG using the ELEGANT program in Section 4. The issues that affect EEHG performance are described in Section 5.

2   Theoretical analysis of storage ring-based EEHG

As seen from EEHG theory (Ref. [1]), the amplitudes of the modulation of EEHG FEL are given by Eq. (2):

$$b_k = 2 \left| \sum_{m=-\infty}^{+\infty} e^{im\phi} J_{-m-k} A_1 [(m+k)B_1 + kB_2] \right.$$
$$\left. \times J_m (kA_2 B_2) e^{-(1/2)[(m+k)B_1 + kB_2]^2} \right|. \qquad (2)$$

Generally, this bunching factor is too complicated to maximise analytically. However, we can use the following approximate formula, Eq. (3), to calculate the bunching factor of the kth order harmonic. Then, the approximate formula of the kth order bunching factor can be written in this form,

$$b_k = \left| J_{k+1}(kA_2 B_2) J_1 [A_1(B_1 - kB_2)] e^{[-\frac{1}{2}(B_1 - kB_2)^2]} \right|. \quad (3)$$

In this equation k is the order of the harmonic number, J_{k+1} is the Bessel function of order $k+1$, and $A_1 = \frac{\Delta E_1}{\sigma_E}$, $A_2 = \frac{\Delta E_2}{\sigma_E}$ are the dimensionless energy derivations. Eqs. (4) and (5) give B_1 and B_2:

$$B_1 = R_{56}^{(1)} k_1 \frac{\sigma_E}{E_0}, \tag{4}$$

$$B_2 = R_{56}^{(2)} k_1 \frac{\sigma_E}{E_0}, \tag{5}$$

where σ_E is the natural energy spread. For HLS-II the natural energy spread is $\sigma_E = 368$ keV, and $k_1 = \omega/c$.

In this paper we use a seeded laser with wavelength 800 nm and aim to radiate in the 31 nm vacuum ultraviolet wave band. Obviously the harmonic number is the 26th harmonic of the seeded laser. The angular frequencies of the two laser beams are $\omega_1 = \omega_2 = 2.35619 \times 10^{15}$. Appropriate dimensionless energy derivation parameters are chosen to be $A_1 = 3$, and $A_2 = 1$.

Now we optimize B_1 and B_2 to maximize the absolute value of the bunching factor shown as Eq. (3). To find the optimal values of B_1 and B_2 which maximize the bunching factor, we maximize the product of $J_{k+1}(kA_2B_2)$ and $J_1[A_1(B_1 - kB_2)]e^{-1/2(B_1 - kB_2)^2}$. This can be realized by maximizing each of the terms. For the first term the corresponding value that maximizes $J_{27}(26A_2B_2)$ is 29.3, so that we get $B_2 = 1.1266$. For the second term the corresponding value that maximizes $J_1[A_1(B_1 - kB_2)]e^{-1/2(B_1 - kB_2)^2}$ is 0.55; this means $B_1 - 26 \times B_2 = 0.55$. So we get $B_1 = 29.8416$. The optimal values of $R_{56}^{(1)}$ and $R_{56}^{(2)}$ from Eq. (4) and Eq. (5) are $R_{56}^{(1)} = 8.259 \times 10^{-3}$m and $R_{56}^{(2)} = 3.128 \times 10^{-4}$m. For an electron storage ring the R_{56} is approximately equal to the product of the momentum compaction factor and the circumference, as shown in Eq. (1). So we find the optimum momentum compaction factor for 26th harmonic EEHG at HLS-II is $\alpha = 1.253 \times 10^{-4}$.
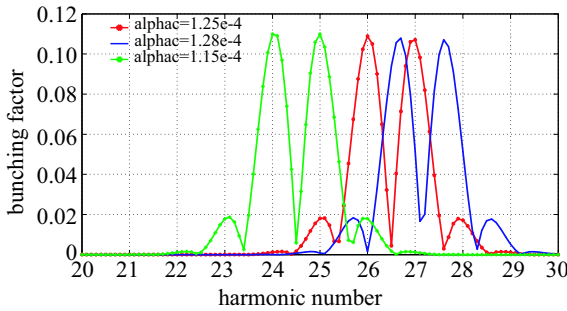
Fig. 2.   (color online) The 26th harmonic bunching factor for different momentum compaction factors. The red line is the bunching factor with $\alpha = 1.25 \times 10^{-4}$, the blue line $\alpha = 1.28 \times 10^{-4}$, and the green line $\alpha = 1.15 \times 10^{-4}$.

As follows from Eq. (3), when the momentum compaction factor is slightly changed, the bunching factor decreases quickly. The 26th harmonic bunching factor with different momentum compaction factors is drawn in Fig. 2.

The results show that the momentum compaction factor is a strict constraint on our storage ring lattice design. A more precise determination of the analysis is listed in Table 2.

Table 2.   The main parameters of 26th harmonic EEHG at HLS-II from the theoretical analysis.

parameter	value
seeded laser wavelength/nm	800
seeded laser power1/MW	2340
seeded laser power2/MW	310
modulator length/m	1.0
modulator period	10
undulator peak field/T	0.93589
energy spread	0.000466
$R_{56}^{(1)}$/mm	8.259
$R_{56}^{(2)}$/mm	0.3127
radiation wavelength/nm	31

3   HLS-II storage ring lattice design for EEHG dispersion relation

As shown in Fig. 1, the EEHG FEL consists of two modulators. Particularly, in our design the two modulators are operated with the same undulator, while the two chicanes of the traditional EEHG are replaced by the structure of the storage ring itself. This is possible because the beam passes repeatedly through the storage ring, compared to the single-pass of a linear accelerator. A practical design scheme of the proposed storage based EEHG FEL at HLS-II is shown in Fig. 3.
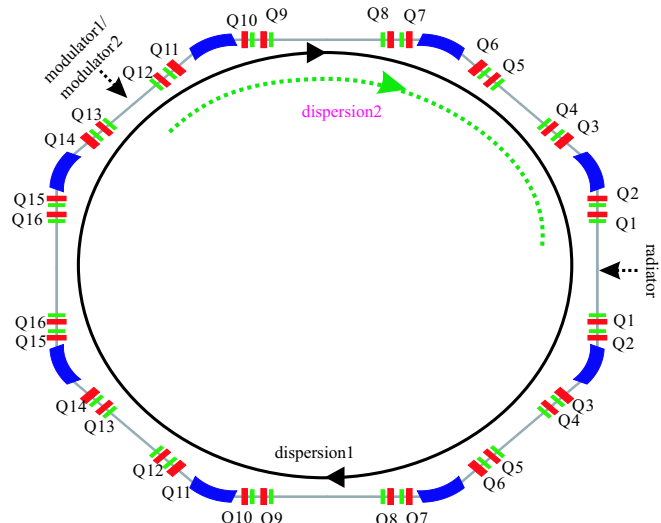
Fig. 3.   (color online) Possible application of the proposed EEHG scheme at the HLS-II storage ring.

As shown in Fig. 3, the two modulators (in fact one undulator) are placed at one of the short straight sections (2.83 m), which is between quadrupole Q13 and Q12, while the radiator is placed at one of the long straight sections (4.51 m), which is 24.8 m away from the modulators. Typically, the short straight section is large enough for modulator installation and the long straight section is large enough for radiator saturated-output. As can be seen from Fig. 3, an electron beam with an average energy E_0 interacts with the seeded laser of frequency ω_1 at modulator 1, and the electron beam energy is modulated. Then the modulated beam goes through the first dispersion section, which means traveling through the whole storage ring, where the energy modulation becomes a longitudinal coordinate modulation. Following the beam passage through the undulator again, the laser power will change from modulator 1 to modulator 2 as shown in Fig. 3. After that the beam goes through dispersion 2, which is part of our storage ring with a length of 24.8 m. Finally, the beam passes through the radiator and radiates a 31 nm wave at vacuum ultraviolet wavelengths.

To demonstrate the storage ring lattice design for 26th harmonic EEHG superradiant undulator radiation, we do not change the magnet structures and just change the quadrupole strengths to meet the requirement of 26th harmonic EEHG as analyzed in the above section.

The present HLS-II is a DBA structure, which means that there are only four independent quadrupoles per superperiod. Furthermore, there are only four independent quadrupoles on the whole ring. As can be seen from Fig. 3, if the four quadrupoles are confirmed, the whole ring's dispersion strength as well as the strength of dispersion 2 are all verified. Clearly, it is hard to satisfy the 26th harmonic EEHG dispersion relation. We overcome this by changing the superperiod from four periods to one superperiod, and release more variables (quadrupole strengths) to meet the two dispersion relations. Then, 16 quadrupoles (see Fig. 3) need to be independently varied to get a satisfactory dispersion relation.

First, we design dispersion section 2, shown in Fig. 3 by the green dotted line. It is composed of twelve quadrupoles and three bending magnets. Of course that means part of the storage ring's dispersion function has to meet the requirement of the second dispersion relation. More precisely, $R_{56}^{(2)}=3.128\times10^{-4}$m is the analytical result given by Section 2. In addition, the linear matrix elements of $R_{51}^{(2)}$ and $R_{52}^{(2)}$ are as low as possible to get a clear strip line at the exit of the second dispersion function. Tracking results show that when $R_{51}^{(2)}$ and $R_{52}^{(2)}$ at the level of 10^{-6}m and 10^{-4}m, the energy strip bands appear. Also, the objective value of $R_{56}^{(2)}$ is a small quantity which means this section is an achromatic section. The achromatic condition of dispersion 2, the $R_{56}^{(2)}$, is determined by the quadrupoles, Q10-Q3, between the bending magnets. So that these eight quadrupole strengths are varied to meet the $R_{56}^{(2)}$ requirement, while the two elements $R_{51}^{(2)}$ and $R_{52}^{(2)}$ are as low as possible. After obtaining the Q10-Q3 strengths the $R_{56}^{(2)}$ is fixed, then the Q11 and Q12 quadrupole strengths are varied to minimize $R_{51}^{(2)}$ and $R_{52}^{(2)}$, while $R_{56}^{(2)}$ is not affected. The two quadrupoles Q1 and Q2 at the outer end of the dispersion section do not affect the dispersion 2 relation used in EEHG, so their strengths will be determined later. Optimization of these quadrupole strengths is complex. We obtain them with the intelligent algorithm reported in our previous work [11]. Finally, we get a dispersion function which meets the analytical result, as shown in Fig. 4.
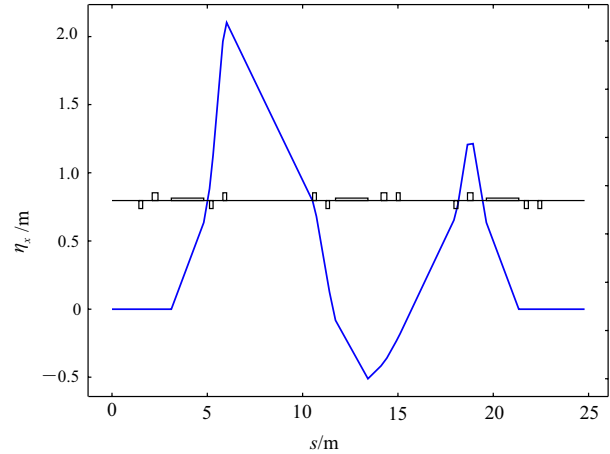

Fig. 4.   (color online) The second dispersion of EEHG at the HLS-II storage ring.

To design the dispersion section 1, which is the whole storage ring's dispersion function, we note that, if both $R_{51}=0$ and $R_{52}=0$ all around the storage ring, the horizontal tune is exactly equal to an integer (see appendix). Fortunately, R_{51} and R_{52} are functions of the distance. Hence, we reduce R_{51} and R_{52} only at the long straight section, as shown in Fig. 3, where modulators are implemented, while their values can be arbitrarily set to other positions. This will help us avoid the integer resonance of the horizontal tune.

The storage ring-based EEHG scheme at the HLS-II storage ring requires that the momentum compaction factor be minimized to 1.253×10^{-4} (or $R_{56}^{(1)}=8.259$ mm) as in the above analysis. The current momentum compaction factor of the HLS-II lattice is 0.0205. So, we need to further minimize the momentum compaction factor for EEHG to maximize the bunching factor. This low momentum compaction factor lattice with small R_{51} and R_{52} is realized by introducing negative dispersion at the middle of these dipoles, while the outer ends of these dipoles are zero for the achromatic condition. As shown in Fig. 3, the Q12 to Q3 quadrupole values are fixed for dispersion 2, and now we vary the remaining quadrupole

strengths to satisfy the dispersion 1 relation. As with the $R_{56}^{(1)}$ requirement, $R_{51}^{(1)}$ and $R_{52}^{(2)}$ also have strict constraints. Simulation results show that both $R_{51}^{(1)}$ and $R_{52}^{(1)}$ at the level of 10^{-4}m will have a clear spacing between the adjacent energy bands of the longitudinal phase space. This work is more complex than the traditional chicane design. Because of symmetry of the chicane, R_{51} and R_{52} are always zero. But the storage ring has many quadrupoles between the bending magnets and is not as symmetric as a chicane, so R_{51} and R_{52} cannot automatically be equal to zero and must be deliberately minimized. In addition to this, the whole storage ring's linear matrix element must satisfy the stable beam condition for long term operation, which means that the linear matrix elements R_{11}, R_{22}, R_{33}, R_{44} must also be constrained. We do this using the intelligent algorithm as for dispersion 2. As a result, we get the whole ring dispersion function as shown in Fig. 5.
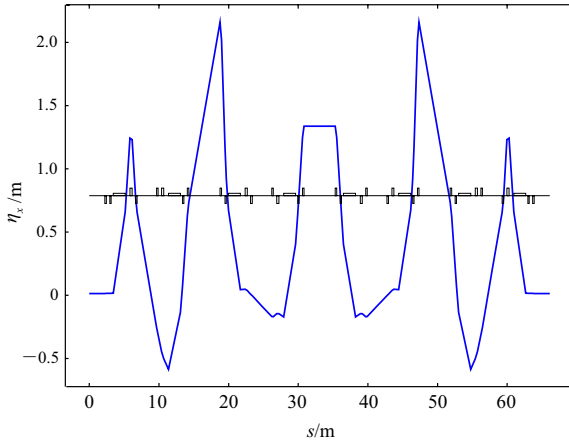
Fig. 5. (color online) The whole ring dispersion function used for dispersion 1 at storage ring EEHG.

Summarizing the above design, we get the group of 16 quadrupole strengths that satisfy the dispersion relation of the storage ring-based EEHG superradiant undulator radiation and the steady operation of the storage ring. The group of 16 quadrupole strengths is listed in Table 3.

Table 3. Quadrupole strengths for storage ring-based EEHG dispersion.

quadrupole strengths for storage ring/m^{-2}			
K_{Q1}	−0.454015	K_{Q2}	−1.345942
K_{Q3}	4.533456	K_{Q4}	−4.145143
K_{Q5}	1.088098	K_{Q6}	0.980978
K_{Q7}	−2.987224	K_{Q8}	3.498510
K_{Q9}	4.738488	K_{Q10}	−4.220283
K_{Q11}	4.728973	K_{Q12}	−3.384838
K_{Q13}	3.086633	K_{Q14}	−1.970773
K_{Q15}	−0.611585	K_{Q16}	3.361993

The main parameters of the lattice are given in Table 4.

Comparing Table 2 with Table 4, the theoretical value of $R_{56}^{(2)}$ is 3.127×10^{-4} m, while the optimized value of $R_{56}^{(2)}$ is $3.1048×10^{-4}$ m. It is complicated for us to optimize $R_{56}^{(2)}$ exactly equal to the theoretical value for the chicane used in classical EEHG. This is because dispersion section 2 is part of the storage ring, so the matrix elements R_{51}, R_{52} should be optimized simultaneously for a clear echo signal. The stability condition for the storage ring lattice also has to be satisfied. This deviation of $R_{56}^{(2)}$ from the theoretical value may degrade the performance of the bunching factor.

Table 4. Optimized parameters for EEHG superradiant undulator radiation simulation at HLS-II storage ring.

parameter	value
momentum compaction factor	$1.253×10^{-4}$
$R_{51}^{(1)}$	$2.0907×10^{-4}$
$R_{52}^{(1)}$	$-9.9110×10^{-4}$ s/kg
$R_{56}^{(2)}$	$3.1048×10^{-4}$ m
$R_{51}^{(2)}$	$-2.5504×10^{-6}$
$R_{52}^{(2)}$	$-4.4722×10^{-4}$ s/kg
tunes	3.663194/3.483192

4 Simulation of EEHG superradiant undulator radiation at HLS-II

4.1 Longitudinal phase space tracking

The process of longitudinal phase space evolution of the storage ring-based EEHG FEL is simulated by the ELEGANT program [12]. In this simulation, the dispersion parameters are taken from Table 4 and modulator parameters are based on Table 2. Due to the limited computation capability we have to use a small number of particles to simulate the real beam. This means that the electron beam should be cut into small pieces, guaranteeing that every piece has a certain number of macro particles. Using part of the beam for simulation can not only reflect the situation of the whole beam but can also save time. We chose a bunch length of 1.5 μm with 200000 particles per bunch for simulation.

Figure 6 shows the evolution of the phase space of the beam as it travels through the system for the parameters discussed above. As shown in Fig. 6, the uniformly distributed particles become energy modulated after modulator 1, then the energy modulation become a distance modulation and the energy strip line can be seen at the exit of the dispersion 1. After that, the modulated beam passes through the second modulator and second dispersion section. The current intensity modulation is shown in Fig. 6(d).
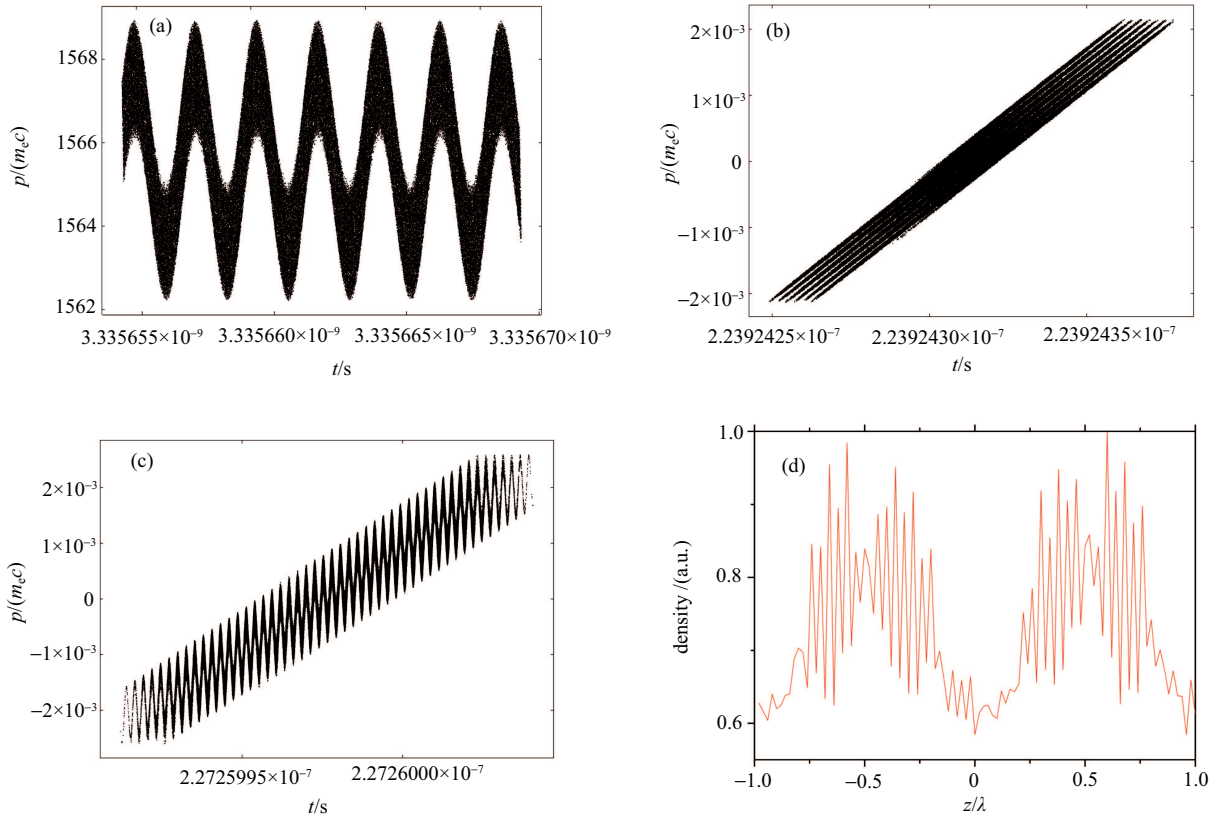
Fig. 6.   (color online) Longitudinal phase space after the beam passes through (a) undulator 1, (b) dispersion 1, and (c) modulator 2. The horizontal axis is the beam longitudinal position and the vertical axis is the particle's momentum with units of m_ec. Plot (d) is the density distribution after the second dispersion.

4.2 Bunching factor simulation

The bunching factor is the most important parameter of EEHG. We also studied the sensitivity of the bunching factor to B_1 and B_2 and to the matrix elements R_{51} and R_{52}. The ELEGANT simulation shows that the maximum bunching factors are not at the point where the analytical result is. Instead the parameters should be slightly adjusted to get the bunching factor, for example, $R_{56}^{(1)}$ is 8.041 mm. The maximum bunching factor at the 26th harmonic is close to 0.1. The result is plotted in Fig. 7. From the picture we see that high coherent EEHG signal can be produced from 800 nm seeded laser at the HLS-II storage ring.

4.3 Peak current and radiation power

The electron beam circulates around the storage ring repeatedly and it must overcome all instabilities for long-term operation. Consequently, the peak current of the beam as well as the radiation power are much lower than for linac-based EEHG. We use the microwave instability, which mainly limits the current of the storage ring, to estimate the average beam current. As shown in Ref. [13], the current threshold of microwave instability can be expressed as follows,

$$I_b > \frac{8\pi^2 \xi^{\text{th}}(\chi)\sigma_z^{7/3}V_{\text{rf}}\cos(\phi_s)f_{\text{rf}}f_{\text{rev}}}{c^2 Z_0 \rho^{1/3}}, \tag{6}$$

where f_{rev} is the revolution frequency, f_{rf} is the RF frequency, V_{rf} is the RF voltage, and ρ is the bending radius. Based on the bunched beam theory, the scaled current $\xi^{\text{th}}(\chi)=0.5+0.34\chi$. The impedance of free space
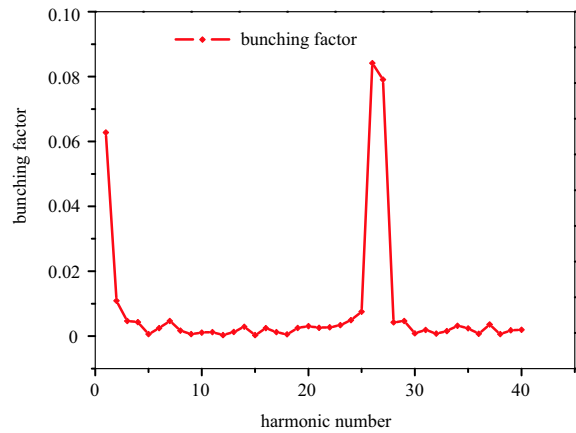

Fig. 7.   (color online) Bunching factor at various wavelengths.

$Z_0 = 120\pi\Omega$. In order to get considerable radiation power, we use a new group of RF parameters instead of the original HLS-II RF cavity parameters. The new RF parameters are $f_{\rm rf} = 612$ MHz and $V_{\rm rf} = 20$ MV, which can be achieved by multi-cell superconducting technology. So, we find that the single bunch current threshold of the newly designed lattice is about 0.028 mA and bunch length is 0.075 mm. Shortening of bunch length is beneficial for the enhancement of peak current.

The relationship between peak current and average current for a Gaussian distributed beam can be expressed as Eq. (7) [14],

$$I_{\rm peak} = I_{\rm avg} \frac{2\pi\overline{R}}{\sqrt{2\pi}\sigma z}. \tag{7}$$

Finally, we get that the peak current of a single bunch is about 10 A which is much lower than a linear accelerator. This is the weakness of storage ring EEHG compared to linac-based EEHG.

The radiation power including coherent and incoherent radiation of a certain frequency can be expressed as the following [15],

$$P_{\rm total} = N_{\rm e} P_0 [1 + (N_{\rm e} - 1) b^2(f)], \tag{8}$$

where $N_{\rm e}$ is the number of particles per bunch, P_0 is the incoherent radiation power, and $b(f)$ is the bunching factor for a certain frequency. In EEHG mode the number of particles $N_{\rm e} = 3.8 \times 10^7$ and the bunching factor $b(f) = 0.08$. In spontaneous emission mode the number of particles $N_{\rm e} = 9.2 \times 10^9$ and bunching factor $b(f) = 0$. Taking the above value into Eq. (8), we find that the radiation power from EEHG is 1000 times higher than the spontaneous radiation power.

For comparison, we simulated the average radiation power by Genesis for both spontaneous emission and EEHG radiation. The result is shown in Fig. 8.
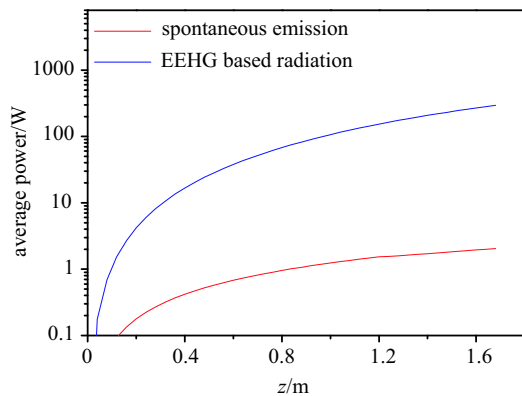

Fig. 8. (color online) Average radiation power from EEHG and spontaneous emission. The red line is the spontaneous emission and the blue line is the EEHG radiation.

From Fig. 8 we see that the average radiation power from EEHG at a distance of 1.8 m can reach 1 kW, which is about three orders of magnitude higher than the spontaneous radiation power. This simulation result agrees with the above analysis.

The main impact of the radiator on the echo signal is the energy spread. However, because of the relatively low peak current of the electron beam and the limited drift space for radiator installation, the radiation cannot reach the high gain segment. The growth of the energy spread caused by the radiator is therefore acceptable and the beam remains stable.

5 Issues that affect EEHG performance

In order to find the RF cavity impact on the separated energy bands, we carried out simulation with ELEGANT including the RF cavity. The simulation results show that when the RF voltage increased to 250 MV the phase space is smeared out. Note that this voltage is 1 order of magnitude higher than the operating voltage. Furthermore, the RF frequency impact on the phase space modulation was also simulated. The results show that when the RF frequency is increased to 204×10^5 MHz the energy bands smear out gradually. This frequency is much higher than the operating frequency. This means that the RF cavity impact on the modulated beam is negligible.

Quantum fluctuations in the process of ISR (Incoherent Synchrotron Radiation) lead to diffusion of energy. If the energy diffusion caused by the ISR effect exceeds the two adjacent energy bands of the longitudinal phase space, the fine structure of the stripe line between the two energy bands is smeared out and thus the echo performance is degraded. The energy spread caused by the ISR effect can be calculated by the following [16],

$$\Delta\sigma_E^2|_{\rm ISR} = \frac{55 e^2 \hbar c}{48\sqrt{3}} \frac{L}{\rho^3} \gamma^7, \tag{9}$$

where $\hbar$ is the Planck constant, c is the speed of light, L is the bending magnet length, ρ is the bending radius and γ is the normalized energy.

Taking the HLS-II parameters (listed in Table 1) into Eq. (9), we find that the energy spread caused by the ISR effect is 1.2 keV.

The two adjacent energy bands can be calculated by numerically solving the following equation [16],

$$[1 + A_1 B_1 \cos(B_1 p)][p + A_1 \sin(B_1 p)] = 0. \tag{10}$$

With the parameters given in the echo scheme $A_1 = 3$, $B_1 = 29.8416$, we get that the smallest energy band between two adjacent energy bands is $0.053\sigma_E = 19.5$ keV. It is clear that the energy band is much larger than the ISR-caused energy spread.

The main concern for dispersion section 2 is the CSR effect. When the beam passes through the dispersion section, the CSR effect may cause additional density modulation and then result in distortion of the echo modulation. For HLS-II, all of the dipole magnets have the same lengths and bending radius, so we can use the final gain of density modulation in a chicane (see Ref. [17] Eq. (38)) to estimate the CSR effect in dispersion 2. The final gain of density modulation in this design is shown in Fig. 9.
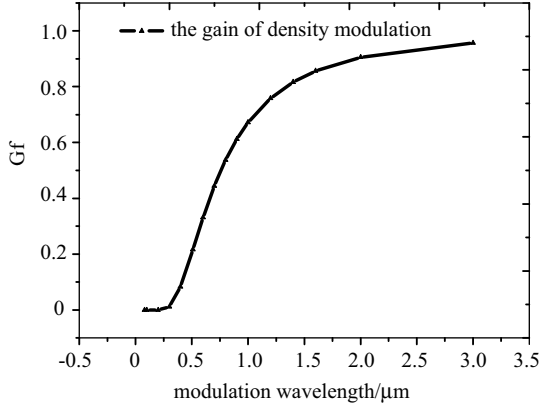

Fig. 9.   Gain of density modulation caused by the CSR effect.

The gain of density modulation is nearly zero when the radiation wavelength is shorter than 0.30 μm. Therefore, the density modulation caused by the CSR effect is negligible for the radiation wavelength designed in this paper.

6   Discussion

In this paper, we have presented a storage ring EEHG superradiant undulator radiation design for the HLS-II.

The 800 nm seeded laser radiates at the 26th harmonic and a 31 nm vacuum ultraviolet spectrum is obtained. We first analyzed the theoretical parameters that maximize the bunching factor of the 26th harmonic. Following that, we designed a storage ring lattice which satisfies the dispersion relation of the EEHG superradiant undulator radiation. Moreover, we demonstrated the process of the longitudinal phase space evolution, and the bunching factor. The issues that affect EEHG performance were also analyzed. In addition to this, the relatively larger dispersion function and nonlinear beam dynamics may reduce the momentum aperture and off-momentum dynamic aperture for storage ring operation. The dynamic aperture is mainly determined by the strengths of nonlinear magnets such as sextupoles, and this is a strict issue for ultra low emittance lattices. We can estimate that the dynamic aperture should be large enough. Of cause momentum aperture is also an important issue which is closely related to sextupole strength and dispersion function. Compared with the present HLS-II storage ring, whose maximum dispersion function is 1.2 m, the maximum dispersion function of the newly designed lattice is 2.2 m. Meanwhile, the energy spread caused by ISR and CSR effects are negligible, as shown in the above analysis. We can estimate that the momentum aperture of the new lattice will also be large enough. These parameters are insufficient for practical application, however. A real start-to-end simulation which includes the tracking of electrons with the desired lattice (nonlinear beam dynamics and CSR effect) and superradiant undulator radiation should be considered in future work. More careful optimization might lead to further improvements of the scheme.

Appendix

When both $R_{51} = 0$ and $R_{52} = 0$, the real part of the following integral vanishes for arbitrary ψ_{s0} [18],

$$0 = \boldsymbol{R}\left\{ \int_{s_0}^{C+s_0} \frac{\sqrt{\beta}}{\rho} e^{i[\psi(s)-\psi(s_0)]} ds \right\}. \tag{A1}$$

All betatron parameters are horizontal and C is the circumference. This means that the following integrals are equal for arbitrary ψ_{s_0},

$$\int_0^C \frac{\sqrt{\beta}}{\rho} e^{i\psi(s)} ds = \int_{s_0}^{C+s_0} \frac{\sqrt{\beta}}{\rho} e^{i\psi(s)} ds. \tag{A2}$$

This means,

$$(1 - e^{i2\pi\nu}) \int_0^{s_0} \frac{\sqrt{\beta}}{\rho} e^{i\psi(s)} ds = 0. \tag{A3}$$

This is because $\psi(s+C) = \psi(s) + 2\pi\nu$. But the integral from $s=0$ to s_0 cannot be zero for arbitrary s_0 (otherwise $\frac{\sqrt{\beta}}{\rho} = 0$). Hence,

$$(1 - e^{i2\pi\nu}) = 0. \tag{A4}$$

This means ν is an integer.

References

1 G. Stupakov. Phys. Rev. Lett., **102**: 074801 (2009)
2 D. Xiang, E. Colby, M. Dunning, et al, Phys. Rev. Lett., **108**: 024802 (2012)
3 D. Xiang, E. Colby, M. Dunning et al, Phys. Rev. Lett., **105**: 114801 (2010)
4 E. Hemsing, M. Dunning, C. Hast et al, Phys. Rev. ST Accel. Beams, **17**: 070702 (2014)
5 E. Hemsing, M. Dunning, B. Garcia et al, Nature Photon., **101**: 1–4 (2016)
6 Z. T. Zhao, D. Wang, J. H. Chen et al, Nature Photon., **6**: 360–363 (2012)
7 R. Molo, M. Höner, H. Huck et al, EEHG and Femtoslicing at DELTA, *Proceedings of FEL2013*, New York, NY, USA (2013)
8 C. Evain, M. E. Couprie, J. M. Filhol et al, Study of High Harmonic Generation at Synchrotron SOLEIL Using Echo Enabling Technique, *Proceedings of IPAC' 10*, Kyoto, Japan (2010)
9 J. Krzywinski, J. T. Delor, P. A. Montanez et al, Design Challenge and startegy for the LCLS-II high repetition rate X-ray FEL photon stoppers, *Proceedings of FEL2015*, Daejeon, Korea (2015)
10 G. West and R. Coffee, Optical Tailoring of xFEL beams, SLAC-TN-15-090
11 W. W. Gao, L.Wang, W. Li, Phys. Rev. ST Accel. Beams, **14**: 094001 (2011)
12 M. Borland, User's manual for elegant program version 29.1.0.
13 Y. H. Cai, Theory of Microwave instability and coherent synchrotron radiation in electron storage rings, *Proceedings of IPAC2011*, San Sebastián, Spain (2011)
14 H. Wiedemann, Particle accelerator physics, Springer, 1999
15 H. T. Li, Y. L. Lu, Z. G. He et al, J Infrared Milli Terahz Waves, **37**: 649–657 (2016)
16 Dao Xiang and Gennady Stupakov, Phys. Rev. ST Accel. Beams, **12**: 030702 (2009)
17 Zhirong Huang and Kwang-Je Kim, Phys. Rev. ST Accel. Beams, **5**: 074401 (2002)
18 Private communication with Yokoya